Materials Science and Engineering C 59 (2016) 203–212

Contents lists available at ScienceDirect

Materials Science and Engineering C

journal homepage: www.elsevier.com/locate/msec

Determining the mechanical properties of electrospun poly-ε-caprolactone (PCL) nanofibers using AFM and a novel fiber anchoring technique

Stephen R. Baker, Soham Banerjee, Keith Bonin, Martin Guthold *

Department of Physics, Wake Forest University, Winston-Salem, NC 27109, United States

ARTICLE INFO

Article history:
Received 18 January 2015
Received in revised form 7 September 2015
Accepted 28 September 2015
Available online xxxx

Keywords:
Atomic Force Microscopy
Nanofibers
Mechanical properties
Polycaprolactone

ABSTRACT

Due to its low cost, biocompatibility and slow bioresorption, poly-ε-caprolactone (PCL) continues to be a suitable material for select biomedical engineering applications. We used a combined atomic force microscopy (AFM)/optical microscopy technique to determine key mechanical properties of individual electrospun PCL nanofibers with diameters between 440–1040 nm. Compared to protein nanofibers, PCL nanofibers showed much lower adhesion, as they slipped on the substrate when mechanically manipulated. We, therefore, first developed a novel technique to anchor individual PCL nanofibers to micrometer-sized ridges on a substrate, and then mechanically tested anchored nanofibers. When held at constant strain, tensile stress relaxed with fast and slow relaxation times of 1.0 ± 0.3 s and 8.8 ± 3.1 s, respectively. The total tensile modulus was 62 ± 26 MPa, the elastic (non-relaxing) component of the tensile modulus was 53 ± 36 MPa. Individual PCL fibers could be stretched elastically (without permanent deformation) to strains of 19–23%. PCL nanofibers are rather extensible; they could be stretched to a strain of at least 98%, and a tensile strength of at least 12 MPa, before they slipped off the AFM tip. PCL nanofibers that had aged for over a month at ambient conditions became stiffer and less elastic. Our technique provides accurate nanofiber mechanical data, which are needed to guide construction of scaffolds for cells and other biomedical devices.

1. Introduction

Synthetic biomaterials have steadily come to the forefront of application-driven design in tissue and biomedical engineering over the past 15 years [1–3]. The increasing use of electrospinning has been one of the reasons for this trend [4]. Electrospinning involves dissolving a polymer, natural or synthetic, in a highly volatile solvent, exposing the solution to a high voltage, and collecting the resulting dry, polymer fibers onto a grounded substrate. The electrospun fibers can be collected in various forms such as sheets or tubes for use in engineering skin grafts, blood vessels, heart valves, tendons and muscles, or as single fibers [5–10]. Recently, the electrospinning process has also been used to fabricate metal/polymer composite fibers [11–13], cell/polymer composite fibers [14] and polymer composite fibers [15] for different applications.

Naturally occurring polymers such as collagen and fibrinogen are well suited for various in vivo applications, promoting cell adhesion and growth by mimicking key mechanobiological and biochemical features of the native extracellular matrix [16–21]. However, scaffolds fabricated from collagen alone exhibit poor viscoelastic properties and break down quickly in buffer unless the sample is crosslinked [22,23]. While our recent studies demonstrate the superior mechanical performance of electrospun fibrinogen nanofibers, problems persist with fast degradation rates and mechanical instability when these fibers are uncrosslinked [18,19,24–26]. Native proteins, such as collagen and fibrinogen, are also more expensive and more difficult to source than synthetic polymers. Such obstacles motivate the need to engineer scaffolds that have good bioresorbability, suitable mechanical properties, reduced biodegradability, easy sourcing and low cost.

Electrospinning synthetic polymers offers an efficient, highly scalable route towards creating bioengineered scaffolds with tailored degradation kinetics, excellent mechanical integrity, and surface functionalization [27–33]. Though polymers such as polyglycolide (PGA) and poly D,L-lactide (PDLA) are common tissue scaffolding materials, here we will focus on poly-ε-caprolactone (PCL). PCL has a slower degradation rate and distinct rheological and viscoelastic properties, making it suitable for specific long term implantation [3,34]. Renewed interest in PCL may be attributed to a growing need for low cost polymers that have specific mechanical properties, are nonimmunogenic, and resorb naturally at a time scale of months and years, far longer than aliphatic polyesters designed for similar uses. Past biomedical applications for PCL include drug delivery sutures, wound dressings, as well as fixation devices [7,35–37]. Other studies have focused on using

* Corresponding author.
E-mail address: gutholdm@wfu.edu (M. Guthold).

http://dx.doi.org/10.1016/j.msec.2015.09.102
0928-4931/

PCL for repair and replacement of bone, ligament, tendon and blood vessels [5,6,38–40]. To better understand how these applications will perform under the stresses and strains encountered in the body, we need to understand the nano- and micro-mechanical properties of the fibers that will be the building blocks of purely synthetic, or hybrid polymer/protein, scaffolds.

In the past, our lab has investigated the mechanical properties of single electrospun fibrinogen fibers (wet [41] and dry [42]) and single electrospun collagen fibers [43], and single fibrin fibers [44,45]. Broadly speaking, wet electrospun fibrinogen and native fibrin fibers are very extensible, as they can be stretched to a maximum strain, ε_{max} of over 100% without breaking, and they have a stiffness (total modulus) on the order of tens (native fibrin) to hundreds (electrospun fibrinogen) of MPa. Dry electrospun fibrinogen fibers are also very extensible ($\varepsilon_{max} > 100\%$), but they are stiffer with a modulus of ~4 GPa. In contrast, native collagen fibers and dry, electrospun collagen fibers have low extensibility ($\varepsilon_{max} < 35\%$), and a higher modulus on the order of several GPa.

In this study, we determined a set of key mechanical properties for electrospun PCL fibers, including viscoelasticity, yield point stress and strain, relaxation times, total and elastic tensile modulus, and energy loss with increasing strain and we show that certain mechanical properties are dependent on sample age. Compared to other native and electrospun single nanofibers, dry electrospun PCL fibers most closely resemble wet, native fibrin fibers, as both are very extensible ($\varepsilon_{max} >$ 100%), rather elastic, and rather soft with a modulus on the order of 10 MPa (wet fibrin fibers) and 60 MPa (dry electrospun PCL fibers).

Thus, electrospun PCL fibers might be particularly well suited for applications requiring biocompatible, slowly resorbed, extensible, relatively soft fibers, at low cost, and with easy sourcing.

2. Materials and methods

2.1. Electrospinning of aligned PCL nanofibers

PCL (Lactel Absorbable Polymers, Inherent Viscosity 1–1.3 dL/g in chloroform, molecular weight (MW) ~120,000–300,000 g/mol) was dissolved in 1,1,1,3,3,3-hexafluoro-2-propanol (HFP, Sigma Aldrich) to a concentration of 100 mg/mL (10% w/vol) and mixed for 5 h. The PCL concentration and molecular weight are similar or somewhat higher than those used by other groups (see Table 1). We did not determine the solution viscosity, which is known to affect fiber morphology [46]. There may be no continuous fiber formation for very low viscosity solutions, and jets may not be ejected from the polymer solution for very high viscosity solutions. However, we did not observe either of these problems. The solution was placed into a 5 mL syringe (Becton-Dickinson, Franklin Lakes, New Jersey). A 20-gauge blunt needle (CML Supply, LLC) was inserted into the syringe and attached to 10–15 cm of Teflon tubing (Small Parts Inc.). The Teflon tubing connected to a 3 cm piece of hypodermic tubing (Small Parts Inc.) and was placed on a stand as schematically depicted in Fig. 1; the syringe was then placed in a syringe pump (PHD 2000 Infusion Syringe Pump, Harvard Apparatus, Holliston, Massachusetts). A voltage of 20 kV (Spellman High Voltage Electronics) was added to the end of the hypodermic tubing directly to the blunt needle that served as the exit orifice. Striated substrates for sample collection were made using soft lithography and micromolding in capillaries as has been described previously [41]. For uniaxially aligning electrospun fiber arrays perpendicular to the striated substrate, a collector plate with copper tape and a gap in the center was used [47]. Attaching the cover slides to the collector plate, across the gap, allowed for fiber alignment perpendicular to the ridges of the striated substrate. A pump rate of 0.8 mL/h and a working distance of 15 cm were used for all samples.

2.2. Anchoring of nanofibers to microridges using UV-curable optical adhesive

A small drop of NOA-81 optical adhesive (Norland Products, Cranbury, NJ) was used for anchoring single fibers to the ridges on the striated substrate. A 2 μm outer diameter micropipette was attached to the clamp of a three-axis micromanipulator (Sutter MP285, Sutter Instrument, Novato, CA). A 10 μL drop of NOA-81 optical adhesive was placed onto a cover slide adjacent to the striated substrate, as can be seen in Fig. 2. The manipulator was placed above the optical glue drop, lowered down along the z-axis into the optical glue and then raised back up. The clamp incident angle, θ, was held at 20–35° relative to the nanomanipulator bar in order to facilitate the flow of glue into the micropipette and to transport a small amount of glue to the ridges of the striated substrate. The nanomanipulator bar itself was at an angle of about 20° relative to the microscope sample surface, so that the overall angle of the micropipette axis relative to the sample surface was ~40–55°. Once the NOA-81 optical glue was transported to point locations on the fiber using the micropipette manipulator, the substrate with these NOA-81 anchoring sites was cured for 60 s with UV-365 nm light (UVP 3UV transilluminator, Upland CA). This ensured adhesion between the glue anchors and the substrate, which both consist of the same optical adhesive.

2.3. Combined AFM/optical microscopy

PCL single fiber manipulations and force measurements were performed at room temperature using a combined atomic force microscopy/optical microscopy technique as described previously [41–44,48]. Briefly, the AFM (Topometrix Explorer, Veeco Instruments) is positioned above a custom-made stage that allows for isolated movement of the sample in relation to the AFM cantilever. The AFM and stage are placed on top of an inverted optical microscope (Zeiss Axiovert 200, Göttingen, Germany). Sample illumination is provided by the camera light located inside the AFM above the cantilever tip. The AFM cantilever (NSC35/AIBS, force constant 14 N/m, MikroMasch, Wilsonville, OR) position is controlled by the NanoManipulator software (3rd Tech, Chapel Hill, NC) to laterally stretch the fibers at a rate of 300 nm/s. Images used to identify fiber changes and anchoring integrity were collected by a

Table 1
Physical properties of individual, electrospun fibers.

Fiber type	Concentration (% wt/vol)	Molecular weight (KDa)	Diameter (nm)	Ref.
Electrospun PCL fibers (<30 days)	10	120–300	440–1040	This study
Electrospun PCL fibers (>30 days)	10	120–300	440–1040	This study
Electrospun PCL (Lim, 2008)	10	80	200–1300	[50]
	12			
	14			
Electrospun PCL (Tan, 2005)	7.5	80	1100–1700	[9]
Electrospun PCL (Wong, 2008)	–	80	350–2500	[51]
Electrospun PCL (Chew, 2006)	8–12	60	230–5000	[52]
Electrospun PCL (Croisier, 2012)	15	80	250–700	[53]
Dry, electrospun fibrinogen fibers	10	340	30–200	[42]
Dry, electrospun collagen fibers	8	140	200–800	[43]

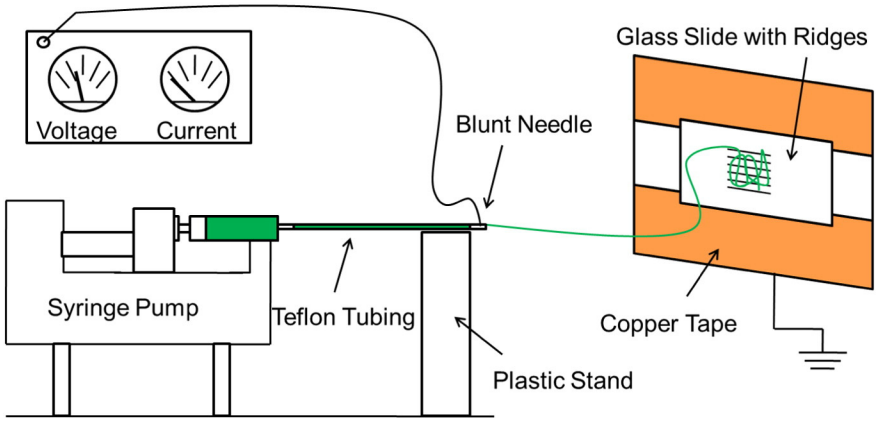

Fig. 1. Electrospinning setup. The spinning parameters were as follows: 20 kV voltage, 0.8 mL/h pump rate and 15 cm working distance between the fixed blunt needle and the copper tape/slide assembly. PCL/HFP solution is indicated in green. The glass slide with ridges is attached to the copper tape collector and grounded. PCL fibers were electrospun for 5–10 s. (For interpretation of the references to color in this figure legend, the reader is referred to the web version of this article.)

Hamamatsu EM-CCD C9100 Camera (Hamamatsu Photonics KK, Japan) and IPlab software (Scanalytics, Fairfax, VA).

2.4. Lateral force, stress, and strain measurements on single fibers

Individual fibers were manipulated by laterally moving the cantilever tip between adjacent ridges and into the fiber as previously described [41–44,48]. This technique is well calibrated as demonstrated by Liu et al. [49]. Lateral force was determined using $F_l = K_C \cdot I_l$, where I_l is the left-right photodiode signal, and K_C is the lateral force constant. The lateral force constant can be found using the Young's modulus of silicon, E (1.69×10^{11} N/m^2), the width, w, length, l, and thickness, t, of the cantilever, the normal force sensor response, S_n, and the height of the cantilever tip, h, by using $K_C = \frac{Ewt^3}{6l^2(h+t/2)} \cdot S_n$. The thickness of the tip can be calculated using the resonance frequency of the cantilever, $f = 0.276 \cdot \sqrt{\frac{Ewt^3}{\rho(\pi \cdot h^3 \cdot l^3 + 2.832 \cdot w \cdot t \cdot l^4)}}$ where ρ is the density of silicon. The width and length of the cantilever, as well as the height of the tip, were found using optical microscope images.

Strain values, ε, were found using $\varepsilon = \frac{L' - L_{initial}}{L_{initial}}$, where L' is half the length of the stretched fiber and $L_{initial}$ is half the initial, unstretched length of the fiber as can be seen in Fig. 3. Stress, $\sigma = \frac{F_{fiber}}{A}$, was calculated by dividing the force on the fiber by the cross-sectional area of the fiber, A. The cross-sectional area, A, was determined using $A = \pi(D/2)^2$, where D, the diameter of the fiber, was found using SEM as described below. The force on the fiber was determined using, $F_{fiber} = \frac{F_l}{2 \sin\beta}$, where F_l is the lateral force as described above and β can be found using the trigonometric relationship between $L_{initial}$ and L', $\beta = \arctan\frac{s}{L_{initial}}$. It should be noted that this assumes a constant fiber radius. The geometry of this set-up can be seen in Fig. 3B.

2.5. Diameter measurements using scanning electron microscopy

Measurements of individual fiber diameter were taken using SEM (Amray 1810, KLA-Tencor). Individual fibers were found by matching images taken from the inverted optical microscope with a 40× lens to the same fiber found on the SEM. Once the fiber was found, an image was taken at 30,000× magnification using the SEM and diameters were measured using the SEM software (EDS2006, IXRF Systems). An average of 15 diameter measurements were taken from each fiber image and all diameter measurements were then averaged to determine the size of each individual fiber.

2.6. Energy loss

Energy loss for individual fibers was calculated using a custom Mathematica® program (details below, Section 3.4). Stress versus strain values were plotted for individual manipulations. During each manipulation the fiber was pulled by the AFM tip to a specific strain and then retracted, back to the starting point. The energy loss is equal to the inscribed area between the forward and backward pulls (Fig. 8A).

When appropriate, all data are reported as the mean value ± standard deviation of the mean.

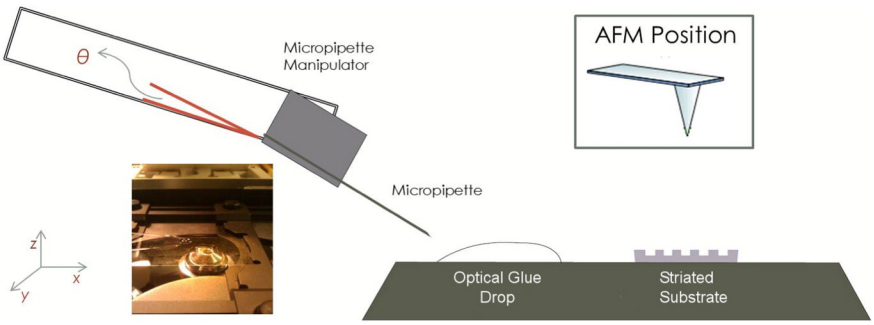

Fig. 2. Fiber anchoring technique. The micropipette attached to the micropipette manipulator is brought down into the optical glue and lifted up. The micropipette is then moved over to the glass slide with ridges (striated substrate). A small drop of optical glue is placed on a fiber that is on top of a ridge. The optical glue is then cured to anchor the PCL fibers to the substrate.

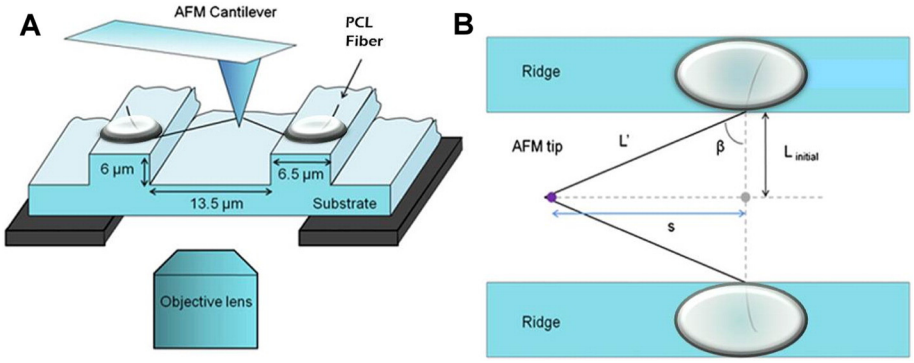

Fig 3. Schematic of single PCL fiber manipulation. The fiber is suspended and anchored to the grooves of the striated substrate. During a manipulation, the AFM probe is moved laterally, thus stretching the fiber. (A) The manipulation is viewed from underneath using an inverted optical microscope. (B) Top view of the fiber and ridges. $L_{initial}$ is half the initial length of the fiber, L' is half the stretched length of the fiber and β is the angle between $L_{initial}$ and L'. The distance the AFM tip travels is indicated by s.
Figure adapted from [42].

3. Results

3.1. Low natural adhesion of PCL nanofibers and anchoring of PCL nanofibers to micrometer-sized ridges

PCL nanofibers demonstrated low natural adhesion and needed to be anchored to the substrate for force measurements. Anchoring of individual PCL fibers was confirmed using optical microscopy images of the fibers before and after manipulations. Fig. 4A and B demonstrate the manipulation of a single unanchored fiber, while Fig. 4C and D display contrasting behavior after manipulating an anchored segment of a fiber. Comparing anchored versus unanchored fiber images, it is evident that the unanchored fiber has moved on the ridges while the anchored fiber segments attached to the ridges are still perpendicular to the ridges of the striated substrate after manipulation. Further investigation of Fig. 4C and D shows that a previously manipulated section of the fiber, designated by red arrows, is unchanged following a later manipulation designated by blue arrows. This indicates that the fiber no longer slips over the ridges following the curing of optical glue anchoring points. Anchoring fibers creates well-defined boundary conditions, which allows for the determination of well-defined fiber mechanical properties.

3.2. Yield point, strain softening and lower limit of maximum extensibility

To determine the mechanical properties of individual, electrospun PCL nanofibers, fibers were electrospun onto a striated substrate with 6.5 μm wide ridges and 13.5 μm wide wells. Individual fibers were anchored to the ridges with optical glue as detailed above. Single fibers were pulled laterally, parallel to the ridges at a continuous rate of 300 nm/s. Optical images were taken from underneath the sample while the AFM tip manipulated individual fibers from above as shown schematically in Fig. 3.

Extensibility is the maximum strain a fiber can withstand before it breaks. Despite numerous attempts, it was not possible to completely rupture any of the PCL fibers with our experimental set-up, like we had routinely done before for other natural (fibrin) and electrospun fibers (wet/dry fibrinogen, dry collagen) [41–44]. The reason for this is that PCL fibers appear to have very little natural adhesive properties, as compared to any of the other, sticky fibers we tested (fibrin fibers, electrospun fibrinogen, electrospun collagen). While anchoring PCL fibers prevents fiber slippage on the striated substrate, at high strain, slippage of the fiber off the AFM tip still occurs during each extensibility measurement. Therefore, it is only possible to give a lower limit for the maximum extension of a PCL fiber. A representative curve of an attempt to determine the extensibility of a PCL fiber can be seen in Fig. 5. Individual fibers were pulled to a maximum strain before they slipped off the AFM tip. The PCL fibers that were pulled did not break, but gave a lower limit for extensibility of 98 ± 30% strain at an average stress of 12 ± 7 MPa. Individual PCL fibers can be pulled to this strain without breaking.

Fig. 5 also shows that these fibers undergo significant strain softening as they are pulled to a maximum stress and strain. Quantitatively we can determine this by calculating the initial slope of the curve and comparing it to the final slope of the curve. The mean value for the initial slope was 28 ± 15 MPa, while the mean value for the final slope was 3.9 ± 3.7 MPa ($p < 0.001$). It should be noted that the latter number assumes a constant fiber cross section throughout the manipulation. Assuming a constant fiber volume, the final slope (modulus) would be about twice as large (~7.8 MPa). The larger initial slope indicates that, on average, PCL fibers undergo strain softening. We also wanted to determine the yield point at which these fibers showed a significant drop in slope. Of the 47 fibers that were pulled, a yield point could be clearly seen in 45 fibers. The mean stress of this yield point was found to be 9.0 ± 6.0 MPa at a strain of 30 ± 11%.

3.3. Elasticity (elastic limit) and modulus measurements

3.3.1. Elasticity

To determine the viscoelastic properties of dry, electrospun PCL fibers we first found the strain at which these fibers were permanently

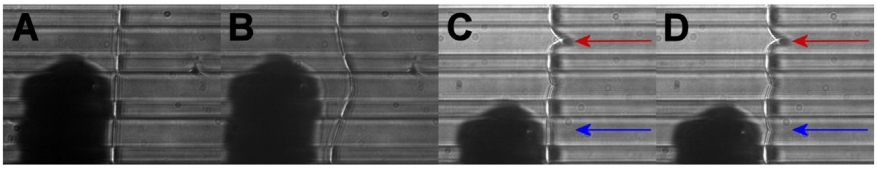

Fig. 4. Confirmation of anchored PCL fibers. (A–B) An unanchored fiber before and after manipulation, respectively. (C–D) An anchored fiber before and after manipulation, respectively. The red arrows in (C–D) indicate a previously manipulated portion of the fiber that was unchanged by the current manipulation, indicated by the blue arrow, demonstrating that the fiber did not slip under the anchoring optical glue. Size of ridges and grooves is 6.5 μm and 13. 5 μm, respectively. (For interpretation of the references to color in this figure legend, the reader is referred to the web version of this article.)

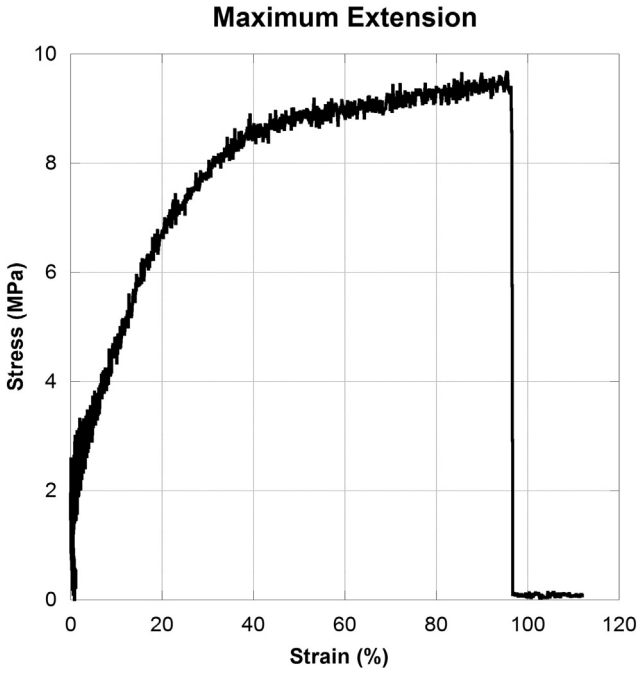

Fig. 5. Maximum extension. Representative curve showing a typical extensibility measurement. A yield point occurs around 30% strain where the slope drastically changes. At 95% strain the fiber slips off the tip (it does not rupture).

deformed (elastic limit). To determine this property, the fiber was pulled to a low strain and then the cantilever was moved back to the starting position which allowed the fiber to return to its initial starting point. Then the fiber was pulled to a slightly larger strain and the stress was removed again (tip returned to starting position). This loading routine was repeated until the fiber was permanently deformed, providing both a lower bound for strain immediately prior to deformation, and an upper bound for strain immediately following deformation. Fig. 6A shows that PCL fibers (<1 month old) had an elastic limit of between 19 ± 5% and 23 ± 6%, i.e., fibers incur permanent damage above this strain.

3.3.2. Modulus (stiffness)

Total and elastic tensile moduli were found using an incremental stress/strain method. To determine these properties, the fiber was stretched to a low, fixed strain, the stretch was halted for approximately a 50 second interval, allowing for stress relaxation, and then the stretch was continued. The process was repeated for increasing strains at roughly the same time intervals, as seen in Fig. 7A and B. Total and relaxed stresses are shown in Fig. 7C. We found the average total tensile modulus for each individual manipulation (initial stress divided by strain), for fibers that are less than one month old, to be 62 ± 26 MPa. The relaxed or elastic tensile modulus for these same individual manipulations (final stress divided by strain), from fibers of the same age, had an average of 53 ± 36 MPa.

In addition to the total and elastic moduli, we were also able to analyze fiber relaxation versus time. By fitting a double exponential equation, $\sigma(t) = \varepsilon_0[Y_\infty + Y_1 \cdot e^{-t/\tau_f} + Y_2 \cdot e^{-t/\tau_s}]$, to each of the relaxation curves, we determined a fast and slow relaxation time, τ_f and τ_s respectively. Here Y_∞ is the relaxed elastic modulus, and Y_0 is the total elastic modulus, $Y_0 = Y_\infty + Y_1 + Y_2$. A representative fit is shown in Fig. 7D. The fast and slow relaxation times for single PCL fibers have average values of $\tau_f = 1.0 \pm 0.3$ s and $\tau_s = 8.8 \pm 3.1$ s respectively. A single exponential function was found to fit the curves less accurately.

3.4. Energy loss

To determine the energy loss for PCL fibers, we performed cyclic loading curves by pulling individual fibers to a low strain with the AFM tip, and then moving back to the unstrained (starting) position. A representative curve is given in Fig. 8A. We analyzed 212 individual cyclical stress vs. strain curves by curve fitting data with a high order polynomial from both forward and backward pulls separately. Integrating the area between both curves, and normalizing with respect to the stretching energy, gives the percentage energy loss. A histogram was generated (Fig. 8B) that shows percentage energy loss as a function of strain interval; increasing strain correlates with increasing percent energy loss. It should be noted that the number of data points used to determine the percent energy loss for each bar shown in Fig. 8B were not the same, they ranged from 54 data points (5–10% strain) to 9 data points (>45% strain).

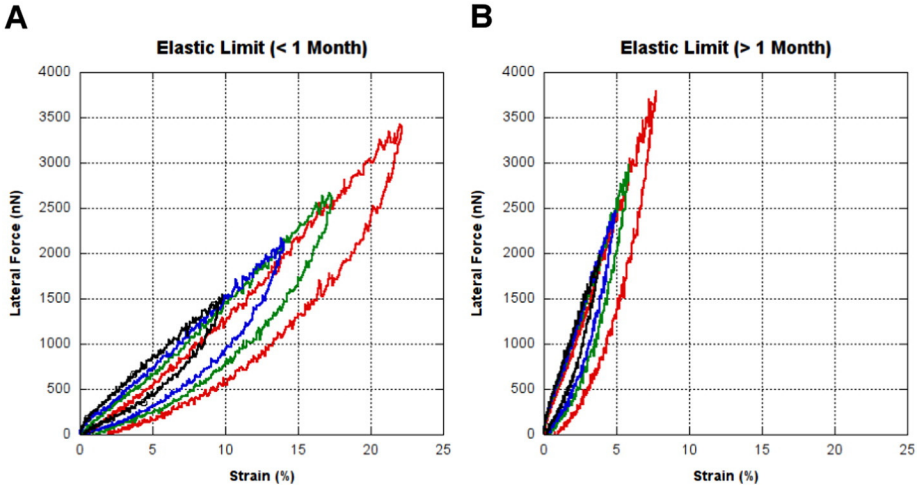

Fig. 6. Elastic limit. Representative curves indicating when a fiber has been permanently deformed. (A) A fiber for a sample that was less than one month old. (B) A fiber for a sample that was greater than one month old. For both A and B, the red curve shows a manipulation that has exceeded the strain at which the fiber can still relax to an unstressed position while the green curve indicates a manipulation that has not yet reached the fiber's elastic limit. The black and blue curves are prior manipulations that have also not yet reached the elastic limit. (For interpretation of the references to color in this figure legend, the reader is referred to the web version of this article.)

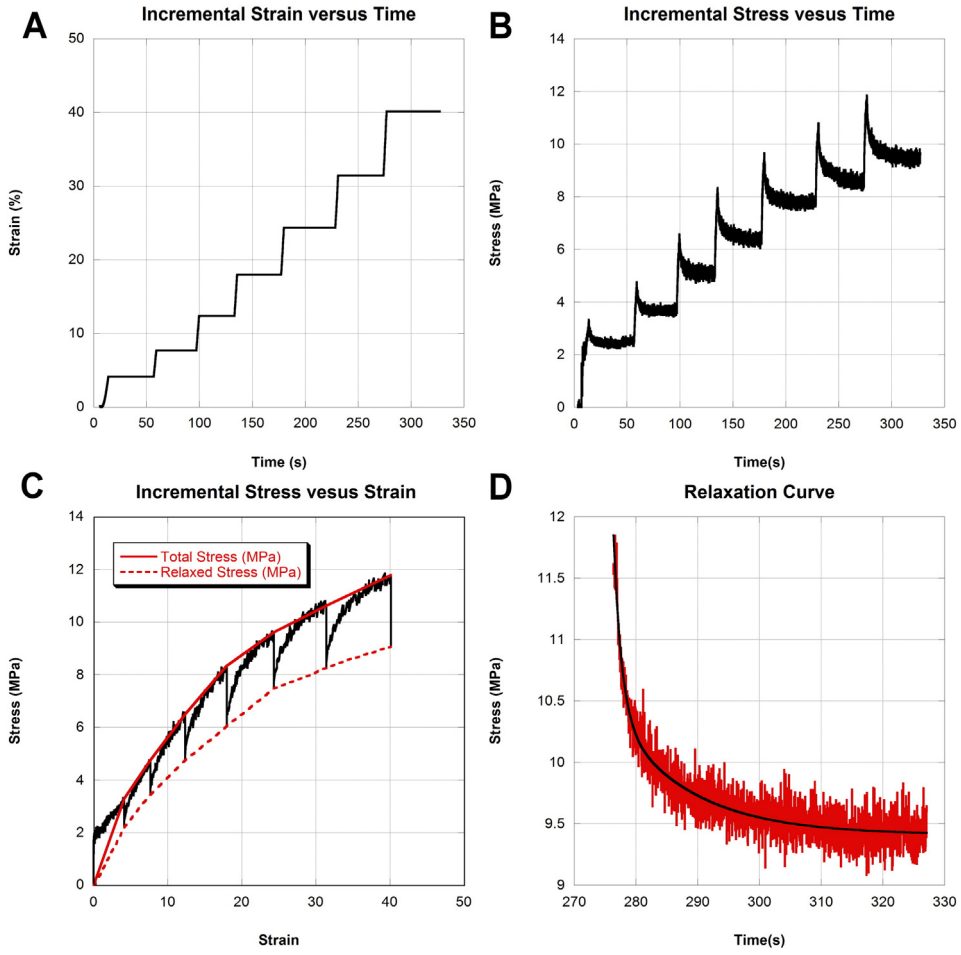

Fig. 7. Sample incremental stress and strain curves. (A) A strain versus time curve emphasizes the various time periods that strain was held constant. (B) A stress versus time curve during the same time period as (A). (A) and (B) show that as strain is held constant the stress relaxes over the same time period. (C) Stress versus strain curve for this time period. The black curve shows the raw data, the solid red line shows the total stress and the red dashed line shows the relaxed or elastic stress. (D) A single relaxation curve from (B) showing the double exponential curve fit. A curve is fit to the raw data from which we can extract total and relaxed moduli as well as fast and slow relaxation times. (For interpretation of the references to color in this figure legend, the reader is referred to the web version of this article.)

3.5. Dependence of mechanical properties on fiber age

We observed a trend in many of the studied mechanical properties as the samples aged. As noted above, the results that have been reported are for samples that were 30 days old or less — defined as the younger sample. Older samples are those that were over 30 days old, and the age of this fiber category ranged from 60 to 90 days old. Age dependence was first observed during elastic limit manipulations. Younger samples had an elastic limit of 19 ± 5% to 23 ± 6% while it was only 6 ± 2% to 8 ± 2% ($p < 0.001$) for the older samples. Age-related changes in

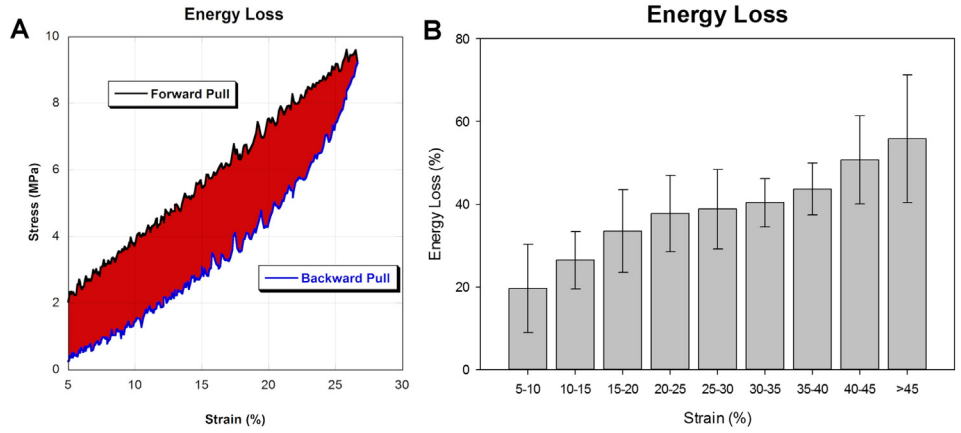

Fig. 8. Energy loss. (A) Representative curve for energy loss. The black (upper) curve corresponds to the forward pull of the cantilever, stretching the fiber. The blue (lower) curve corresponds to the backward motion of the cantilever, returning to the starting position. The red area between the two curves shows the amount of energy lost during this stretching cycle. (B) A histogram of the percentage of energy lost as a function of strain; energy loss increases steadily with increasing strain. (For interpretation of the references to color in this figure legend, the reader is referred to the web version of this article.)

relaxation times were also observed: fast relaxation times increased from $\tau_f = 1.0 \pm 0.3$ for younger samples to $\tau_f = 1.7 \pm 0.4$ s for older samples ($p < 0.001$). Slow relaxation times increased from 8.8 ± 3.1 s for younger samples to 21 ± 9 s for older samples ($p < 0.001$). Age dependence was also observed for the total tensile modulus. Younger samples had a total tensile modulus of 62 ± 26 MPa while older samples had a total tensile modulus of 99 ± 84 MPa ($p < 0.001$). There was no statistically significant difference between the elastic modulus when comparing younger and older samples ($p = 0.161$ Mann Whitney U, $p = 0.006$ t-test). We also did not observe a statistically significant change in maximum extensibility or energy loss with age.

3.6. Statistical analysis

Statistical analysis for samples was done using either an independent t-test or Mann Whitney U test to compare differences with respect to slope (yield point) or age of sample (elastic limit, fast and slow relaxation time, total and elastic modulus).

4. Discussion

We have developed a novel anchoring technique for electrospun fibers that allowed us to determine various mechanical properties of single, electrospun poly-ε-caprolactone (PCL) nanofibers (diameter range: 440 nm–1040 nm). The anchoring efficacy was confirmed using optical microscopy and force data from the AFM cantilever as shown in Fig. 4 and S1 respectively. Unanchored fibers (Fig. 4A and B) easily slip during a mechanical manipulation, while the anchoring points of anchored fibers remain firmly in place during a mechanical manipulation (Fig. 4C and D). Anchoring could also be confirmed by comparing the force-extension curves for unanchored fibers to the force-extension curves for anchored fibers as shown in Fig. S1. For the unanchored fiber the force drops to a lower value multiple times during the manipulation; Fig. S1B shows an increase in force until the fiber slips off the cantilever tip. After samples had been manipulated, we were also able to confirm our anchoring technique using scanning electron microscopy, as shown in Fig. 9. Taken together, these three techniques demonstrate that individual fibers were rigidly anchored to the striated substrate throughout all lateral force measurements. The images in Fig. 9 also show that the glue does not wick along the fiber, which would alter its mechanical properties.

We used a combined atomic force microscopy/optical microscopy technique that was developed in our lab to determine mechanical properties of single electrospun poly-ε-caprolactone (PCL) fibers [42]. We found that PCL fibers have low natural adhesion, causing the fiber to slip off the cantilever tip in our maximum extensibility measurements. Our lower limit value for the extensibility is 98 ± 30%; that is, the fiber could be stretched to this point before it slipped, but it did not yet break. This value is consistent with values found for similar PCL nanofibers. Using a nanotensile tester, Lim and Tan found maximum strain values on the order of about 40%, 100% and 200% for 10 wt.%, 12 wt.% and 14 wt.% PCL nanofibers (MW 80,000 g/mol), respectively, and 200% in an earlier report [9,50]. These authors also found that the extensibility depends on the PCL concentration and fiber diameter. They surmised that fiber crystallinity (which is affected by PCL concentration and fiber diameter) may be the underlying parameter that controls fiber properties such as extensibility and modulus, with higher crystallinity resulting in a stiffer and less extensible fiber. Wong et al. reported an extensibility of between 50% and 90% for PCL nanofibers (MW 80,000 g/mol) with diameters between 350 nm and 1600 nm [51]. Chew et al. found extensibilities of 50% to 100% for PCL nanofibers (8% -12% PCL, MW 60,000 g/mol) [52]. During our manipulations we were able to determine the yield point for electrospun PCL nanofibers, a property that has been difficult to quantify, as a result of smooth transitions from the elastic to the plastic region in previously studied nanofibers. This measurement allows us to determine when strain softening will occur, a property indicative of permanent deformation. The yield point stress (9.0 ± 6.0 MPa) and yield point strain (30 ± 11%) are similar to those found by Tan et al. (13 ± 7 MPa and 20 ± 10% respectively), and Wong et al. (~35 MPa and ~20%, respectively) using different techniques [9,51].

PCL nanofibers show viscoelastic properties. Using incremental stress–strain curves, which had not been used on PCL nanofibers before, we determined a total tensile modulus of 62 ± 26 MPa and elastic tensile modulus of 53 ± 36 MPa. The total tensile modulus may be compared to the tensile modulus determined by other methods. Other teams reported similar, but somewhat higher values of 120 MPa, about 100 MPa–500 MPa in our diameter range, 275 MPa in our diameter range, 1000 MPa–3000 MPa, and 3000 MPa–5000 MPa [9,50–53]. It is not clear why most of these values are higher, but it could be due to technical differences and different nanofiber preparations. Another likely reason is that our fibers were formed from PCL with MW ~120,000–300,000 g/mol, whereas all other nanofibers were formed from PCL with MW 80,000 or 60,000 g/mol. It could be that higher molecular weight PCL results in softer nanofibers. These different values suggest that different nanofiber properties can be achieved by varying the preparation methods. The observation that the elastic tensile modulus in our measurement is only 15% smaller than the total tensile modulus indicates that the viscous component is small for small deformations in PCL nanofibers. The same conclusion can be reached from the small energy loss at small deformation (<20% energy loss for strains <10%). That is, even though electrospun PCL nanofibers show viscoelastic behavior, they can be treated as elastic fibers to a good approximation (<20% error) for small strains (<10%). It has been shown that the tensile modulus varies somewhat with diameter, with thinner fibers having a higher modulus than thicker fibers [9,50,51]. This effect was attributed to thin fibers having a higher crystallinity than thick fibers, and the effect was strongest for fibers smaller than 500 nm. We did not see a pronounced diameter dependence of the tensile modulus over our diameter range (440 nm–1040 nm), Supplementary Fig. S2, probably because our fiber diameters were mostly above 500 nm.

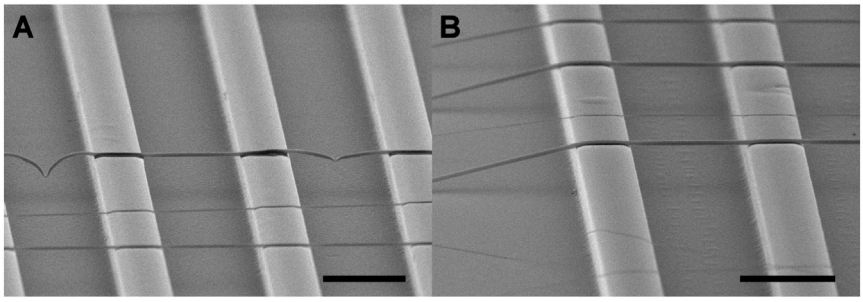

Fig. 9. Scanning electron micrograph images. (A) An image showing a single fiber that has been anchored and manipulated. The figure shows that fibers have been glued to the ridges of the striated substrate and also that the glue has not wicked along the individual fibers. (B) An image showing fibers that have not been anchored or manipulated spanning the ridges of the striated substrate. Scale bars are 10 μm (additional SEM images, see Supplementary material).

Making structures out of electrospun nanofibers typically requires more effort than just molding them from the corresponding bulk material, and the question arises if this extra effort is justified in biomedical engineering. Are structures formed from nanofibers different, and therefore, more suitable and advantageous for some applications as compared to structures formed from bulk material? The answer appears to be yes. For example, it is becoming apparent that cell growth and cell behavior depend on the mechanical and geometric properties of the cell environment (in addition to the biochemical environment) [54–56]. Thus, one goal in tissue engineering is to mimic the structural and mechanical properties of the extracellular matrix, and electrospun nanofibers match the dimensions of fibers in the extracellular matrix well. The micromechanical and microstructural properties of cell substrates do matter, and they can be used to control cell behavior, which points to the importance of investigating and fine-tuning nanofiber mechanical properties.

Devices with identical macroscopic shapes may show different mechanical properties depending on whether they were formed from nanofibers or bulk material; for instance, a specimen formed from PCL nanofibers was stiffer, stronger, and not as ductile as a specimen formed from bulk material [51].

It is also useful to compare PCL nanofiber mechanical properties with the properties of some other, protein-based electrospun nanofibers, since different applications may have different mechanical, structural and biochemical requirements (Tables 1 & 2). Fibrin (activated fibrinogen) polymerizes into a fibrin network, which is the major structural component of a blood clot, and is involved in wound healing. Fibrin fibers are extraordinarily extensible (150%–220% strain) and elastic (50%–100% strain) and have a tensile modulus on the order of 10 MPa [44,45]. Electrospun fibrinogen is thus considered a good candidate for use in biomedical engineering applications requiring soft, extensible fibers. Wet and dry electrospun fibrinogen fibers retain some of the native properties of fibrin fibers, as they are also very extensible (130% (wet); 113% (dry)), however their tensile moduli differ, with the dry fibrinogen fiber modulus being significantly higher (17.5 MPa (wet), 4200 MPa (dry)) [41,42]. Collagen is the most abundant protein in the body and has numerous structural and mechanical functions. For example, it occurs in cartilage, skin, and the extracellular matrix. Native collagen fibrils have low extensibility (< 20% strain) and are relatively stiff with a tensile modulus on the order of 1000 MPa [57]. Dry electrospun collagen fibers have relatively low extensibility, (30% strain) and have a modulus ranging from 200–10,000 MPa [43].

The mechanical properties of electrospun PCL nanofibers do not closely mimic any of the natural or electrospun protein fibers. However, they seem to come closer to fibrin fibers and electrospun fibrinogen fibers, rather than collagen fibers.

The viscoelastic properties of single electrospun PCL fibers were affected by the age of the fiber sample. This is an important property for determining how long a scaffold made from these single fibers can be stored before the mechanical properties are significantly altered. PCL has seen a recent resurgence in biomedical and tissue engineering applications in large part due to a slow degradation time under physiological conditions which is desirable for certain applications [3]. To determine how well a sample will react to mechanical stimulus we need to understand the age at which the mechanical properties of the material change. These viscoelastic properties for single PCL fibers changed for fiber samples that were greater than 30 days old (stored at room temperature); characteristic differences due to aging were first observed when determining the fibers' elastic limit. As noted above, younger samples could be pulled to greater strains, but smaller stresses than older samples. This observation shows that the strains to which a single fiber can be pulled are dependent on the age of the sample. Table 2 shows that the fast and slow relaxation times, as well as the total and elastic moduli, are also dependent on the age of the fiber sample. The aging effect may be due to some annealing occurring at room temperature [58], and might be reduced by storing the fibers at lower temperatures.

The amount of energy lost during individual manipulations was dependent on the strain at which a single fiber was pulled (Fig. 8B). We have previously observed the dependence of energy loss on strain for electrospun type I collagen fibers and single fibrin fibers [43,44]. While energy loss for single electrospun collagen fibers plateaus at 80% at a strain of 12% the energy loss for single PCL fibers is only 56 ± 15% at strains up to 62%. It should be noted that these strains may not be high enough to observe a plateau in energy loss. We have previously shown that crosslinked and uncrosslinked fibrin fibers have an energy loss that does not plateau until greater than 100% strain.

We chose to investigate individual PCL fibers because of their numerous possibilities for use in both biomedical and tissue engineering. Currently, electrospun collagen is widely used due to its low immunogenicity in the human body. However, single electrospun collagen fibers have some undesirable properties that limit their potential use in tissue engineering including low elasticity and extensibility, and low stability when the fibers are uncrosslinked. In contrast, many of the properties found for electrospun PCL are similar to electrospun fibrinogen — see Table 2. PCL may in fact be a better choice than fibrinogen for certain biomedical purposes because of its low cost. In addition, it appears that PCL's viscoelastic properties can be fine-tuned depending on mechanical needs by changing the solution properties, for example, molecular weight or concentration, or by changing the syringe pump rate and/or accelerating voltage. Combining these findings, we believe these data can be used to better design scaffolds that need the specific mechanical and bioresorbable properties of PCL while also motivating the need to better understand the properties of hybrid protein/synthetic polymer electrospun nanofibers.

Table 2
Mechanical properties of individual, electrospun fibers.

Fiber type	ε_{max} (%)	$\varepsilon_{elast.\ limit}$ (%)	τ_f (s)[a]	τ_s (s)[b]	Elastic Mod. (MPa)	Total Mod. (MPa)	Yield strain (%)	Yield strain (MPa)	Ref.
Electrospun PCL fibers (<30 days)	>98 ± 30	19 ± 5 to 23 ± 6	0.98 ± 0.26	8.79 ± 3.08	52.9 ± 36.2	62.3 ± 25.6	30 ± 11	9.0 ± 6.0	This study
Electrospun PCL fibers (>30 days)	>98 ± 30	6 ± 2 to 8 ± 2	1.69 ± 0.44	21.22 ± 8.97	61.4 ± 51.1	99.2 ± 83.9	30 ± 11	9.0 ± 6.0	This study
Electrospun PCL (Lim, 2008)	~40 ~100 ~200	–	–	–	–	–	–	–	[50]
Electrospun PCL (Tan, 2005)	200 ± 100	–	–	–	–	120 ± 30	20 ± 10	13 ± 7	[9]
Electrospun PCL (Wong, 2008)	~50–90	–	–	–	–	275	~20	~35	[51]
Electrospun PCL (Chew, 2006)	50–100	–	–	–	–	1000–3000	–	–	[52]
Electrospun PCL (Croisier, 2012)	–	–	–	–	–	3700 ± 700	–	–	[53]
Dry, electrospun fibrinogen fibers	110	16	1.2	11	3700	4200	–	–	[42]
Dry, electrospun collagen fibers	33	<2	–	–	–	200–10,00	–	–	[43]

[a] τ_f = fast relaxation time.
[b] τ_s = slow relaxation time.

5. Conclusion

We developed a novel method for anchoring micro- and nano-fibers to the microridges of an optical adhesive substrate. A combined atomic force microscopy/optical microscopy technique was then used to determine the mechanical properties of anchored single, electrospun PCL fibers. The anchoring is critical since the fibers do not naturally bind to the substrates well enough to measure key mechanical properties of individual fibers. In fact, PCL seems to have very low natural adhesion, since PCL fibers slipped on the substrate when not anchored, and they slipped off the AFM tip at high strains. PCL fibers may have suitable mechanical properties for various applications in biomedical and tissue engineering including blood vessels, skin grafts, and tendons. Viscoelastic properties were found to depend on the age of the fibers. Younger fibers could be pulled to a greater strain before permanent deformation than older fibers. The relaxation times and total and elastic moduli also showed age-related dependencies. This dependence on age gives us a better understanding of how PCL degrades, from a mechanical perspective, over time. Combining these findings with PCL's bioresorbable properties will allow for better fabrication of specific bioengineered scaffolds and devices.

Acknowledgments

We thank Glen Marrs, director of the WFU Microscopic Imaging Core Facility, for assistance in obtaining the SEM images of the substrates with PCL fibers.

This work was supported by a National Science Foundation Materials and Surface Engineering grant from the Division of Civil, Mechanical, and Manufacturing Innovation (CMMI-1152781) and a grant from the Wake Forest Center for Molecular Communication and Signaling (U01057).

Appendix A. Supplementary data

Supplementary data to this article can be found online at http://dx.doi.org/10.1016/j.msec.2015.09.102.

References

[1] R.R. Duling, R.B. Dupaix, N. Katsube, J. Lannutti, Mechanical characterization of electrospun polycaprolactone (PCL): a potential scaffold for tissue engineering, J. Biomech. Eng. 130 (2008) (011006-011006).
[2] M.P. Lutolf, J.A. Hubbell, Synthetic biomaterials as instructive extracellular microenvironments for morphogenesis in tissue engineering, Nat. Biotechnol. 23 (2005) 47–55.
[3] M.A. Woodruff, D.W. Hutmacher, The return of a forgotten polymer—polycaprolactone in the 21st century, Prog. Polym. Sci. 35 (2010) 1217–1256.
[4] D. Li, Y.N. Xia, Electrospinning of nanofibers: reinventing the wheel? Adv. Mater. 16 (2004) 1151–1170.
[5] M.R. Ladd, S.J. Lee, J.D. Stitzel, A. Atala, J.J. Yoo, Co-electrospun dual scaffolding system with potential for muscle–tendon junction tissue engineering, Biomaterials 32 (2011) 1549–1559.
[6] S.J. Lee, J. Liu, S.H. Oh, S. Soker, A. Atala, J.J. Yoo, Development of a composite vascular scaffolding system that withstands physiological vascular conditions, Biomaterials 29 (2008) 2891–2898.
[7] H.M. Powell, S.T. Boyce, Engineered human skin fabricated using electrospun collagen-PCL blends: morphogenesis and mechanical properties, Tissue Eng. A 15 (2009) 2177–2187.
[8] E.P.S. Tan, C.N. Goh, C.H. Sow, C.T. Lim, Tensile test of a single nanofiber using an atomic force microscope tip, Appl. Phys. Lett. 86 (2005).
[9] E.P.S. Tan, S.Y. Ng, C.T. Lim, Tensile testing of a single ultrafine polymeric fiber, Biomaterials 26 (2005) 1453–1456.
[10] M.I. Van Lieshout, C.M. Vaz, M.C.M. Rutten, G.W.M. Peters, F.P.T. Baaijens, Electrospinning versus knitting: two scaffolds for tissue engineering of the aortic valve, J. Biomater. Sci. Polym. Ed. 17 (2006) 77–89.
[11] K.R. Reddy, V.G. Gomes, M. Hassan, Carbon functionalized TiO_2 nanofibers for high efficiency photocatalysis, Mater. Res. Exp. 1 (2014) 015012.
[12] K.R. Reddy, M. Hassan, V.G. Gomes, Hybrid nanostructures based on titanium dioxide for enhanced photocatalysis, Appl. Catal. A Gen. 489 (2015) 1–16.
[13] K.R. Reddy, K. Nakata, T. Ochiai, T. Murakami, D.A. Tryk, A. Fujishima, Facile fabrication and photocatalytic application of Ag nanoparticles–TiO_2 nanofiber composites, J. Nanosci. Nanotechnol. 11 (2011) 3692–3695.
[14] M. Yeo, G. Kim, Fabrication of cell-laden electrospun hybrid scaffolds of alginate-based bioink and PCL microstructures for tissue regeneration, Chem. Eng. J. 275 (2015) 27–35.
[15] N. Kimura, T. Sakumoto, Y. Mori, K. Wei, B.-S. Kim, K.-H. Song, I.-S. Kim, Fabrication and characterization of reinforced electrospun poly(vinylidene fluoride-co-hexafluoropropylene) nanofiber membranes, Compos. Sci. Technol. 92 (2014) 120–125.
[16] M.Y. Li, M.J. Mondrinos, M.R. Gandhi, F.K. Ko, A.S. Weiss, P.I. Lelkes, Electrospun protein fibers as matrices for tissue engineering, Biomaterials 26 (2005) 5999–6008.
[17] M.J. McClure, S.A. Sell, D.G. Simpson, G.L. Bowlin, Electrospun polydioxanone, elastin, and collagen vascular scaffolds: uniaxial cyclic distension, J. Eng. Fibers Fabr. 4 (2009) 18–25.
[18] M.C. McManus, E.D. Boland, D.G. Simpson, C.P. Barnes, G.L. Bowlin, Electrospun fibrinogen: feasibility as a tissue engineering scaffold in a rat cell culture model, J. Biomed. Mater. Res. A 81A (2007) 299–309.
[19] M.C. McManus, S.A. Sell, W.C. Bowen, H.P. Koo, D.G. Simpson, G.L. Bowlin, Electrospun fibrinogen–polydioxanone composite matrix: potential for in situ urologic tissue engineering, J. Eng. Fibers Fabr. 3 (2008).
[20] H. Wu, J. Fan, C.-C. Chu, J. Wu, Electrospinning of small diameter 3-D nanofibrous tubular scaffolds with controllable nanofiber orientations for vascular grafts, J. Mater. Sci. Mater. Med. 21 (2010) 3207–3215.
[21] I.-S. Yeo, J.-E. Oh, L. Jeong, T.S. Lee, S.J. Lee, W.H. Park, B.-M. Min, Collagen-based biomimetic nanofibrous scaffolds: preparation and characterization of collagen/silk fibroin bicomponent nanofibrous structures, Biomacromolecules 9 (2008) 1106–1116.
[22] L. Buttafoco, N.G. Kolkman, P. Engbers-Buijtenhuijs, A.A. Poot, P.J. Dijkstra, I. Vermes, J. Feijen, Electrospinning of collagen and elastin for tissue engineering applications, Biomaterials 27 (2006) 724–734.
[23] D.I. Zeugolis, S.T. Khew, E.S.Y. Yew, A.K. Ekaputra, Y.W. Tong, L.-Y.L. Yung, D.W. Hutmacher, C. Sheppard, M. Raghunath, Electro-spinning of pure collagen nano-fibres — just an expensive way to make gelatin? Biomaterials 29 (2008) 2293–2305.
[24] M.C. McManus, E.D. Boland, H.P. Koo, C.P. Barnes, K.J. Pawlowski, G.E. Wnek, D.G. Simpson, G.L. Bowlin, Mechanical properties of electrospun fibrinogen structures, Acta Biomater. 2 (2006) 19–28.
[25] S.A. Sell, M.P. Francis, K. Garg, M.J. McClure, D.G. Simpson, G.L. Bowlin, Cross-linking methods of electrospun fibrinogen scaffolds for tissue engineering applications, Biomed. Mater. 3 (2008).
[26] G.E. Wnek, M.E. Carr, D.G. Simpson, G.L. Bowlin, Electrospinning of nanofiber fibrinogen structures, Nano Lett. 3 (2003) 213–216.
[27] V. Beachley, X. Wen, Polymer nanofibrous structures: fabrication, biofunctionalization, and cell interactions, Prog. Polym. Sci. 35 (2010) 868–892.
[28] W. Cui, Y. Zhou, J. Chang, Electrospun nanofibrous materials for tissue engineering and drug delivery, Sci. Technol. Adv. Mater. 11 (2010).
[29] W.J. Li, J.A. Cooper, R.L. Mauck, R.S. Tuan, Fabrication and characterization of six electrospun poly(alpha-hydroxy ester)-based fibrous scaffolds for tissue engineering applications, Acta Biomater. 2 (2006) 377–385.
[30] R. Neppalli, C. Marega, A. Marigo, M.P. Bajgai, H.Y. Kim, V. Causin, Improvement of tensile properties and tuning of the biodegradation behavior of polycaprolactone by addition of electrospun fibers, Polymer 52 (2011) 4054–4060.
[31] G. Ozturk, T.E. Long, Michael addition for crosslinking of poly(caprolactone)s, J. Polym. Sci. A, Polym. Chem. 47 (2009) 5437–5447.
[32] Q.P. Pham, U. Sharma, A.G. Mikos, Electrospinning of polymeric nanofibers for tissue engineering applications: a review, Tissue Eng. 12 (2006) 1197–1211.
[33] A. Tambralli, B. Blakeney, J. Anderson, M. Kushwaha, A. Andukuri, D. Dean, H.-W. Jun, A hybrid biomimetic scaffold composed of electrospun polycaprolactone nanofibers and self-assembled peptide amphiphile nanofibers, Biofabrication 1 (2009).
[34] J. Gunn, M. Zhang, Polyblend nanofibers for biomedical applications: perspectives and challenges, Trends Biotechnol. 28 (2010) 189–197.
[35] C.P. Barnes, S.A. Sell, E.D. Boland, D.G. Simpson, G.L. Bowlin, Nanofiber technology: designing the next generation of tissue engineering scaffolds, Adv. Drug Deliv. Rev. 59 (2007) 1413–1433.
[36] D. Liang, B.S. Hsiao, B. Chu, Functional electrospun nanofibrous scaffolds for biomedical applications, Adv. Drug Deliv. Rev. 59 (2007) 1392–1412.
[37] J. Venugopal, S. Ramakrishna, Biocompatible nanofiber matrices for the engineering of a dermal substitute for skin regeneration, Tissue Eng. 11 (2005) 847–854.
[38] L. Koepsell, L. Zhang, D. Neufeld, H. Fong, Y. Deng, Electrospun nanofibrous polycaprolactone scaffolds for tissue engineering of annulus fibrosus, Macromol. Biosci. 11 (2011) 391–399.
[39] W.J. Li, R. Tuli, C. Okafor, A. Derfoul, K.G. Danielson, D.J. Hall, R.S. Tuan, A three-dimensional nanofibrous scaffold for cartilage tissue engineering using human mesenchymal stem cells, Biomaterials 26 (2005) 599–609.
[40] H. Yoshimoto, Y.M. Shin, H. Terai, J.P. Vacanti, A biodegradable nanofiber scaffold by electrospinning and its potential for bone tissue engineering, Biomaterials 24 (2003) 2077–2082.
[41] C.R. Carlisle, C. Coulais, M. Namboothiry, D.L. Carroll, R.R. Hantgan, M. Guthold, The mechanical properties of individual, electrospun fibrinogen fibers, Biomaterials 30 (2009) 1205–1213.
[42] S. Baker, J. Sigley, C.C. Helms, J.D. Stitzel, J. Berry, K. Bonin, M. Guthold, The mechanical properties of dry, electrospun fibrinogen fibers, Mater. Sci. Eng. C 32 (2012) 215–221.
[43] C.R. Carlisle, C. Coulais, M. Guthold, The mechanical stress–strain properties of single electrospun collagen type I nanofibers, Acta Biomater. 6 (2010) 2997–3003.
[44] W. Liu, C.R. Carlisle, E.A. Sparks, M. Guthold, The mechanical properties of single fibrin fibers, J. Thromb. Haemost. 8 (2010) 1030–1036.
[45] W. Liu, L.M. Jawerth, E.A. Sparks, M.R. Falvo, R.R. Hantgan, R. Superfine, S.T. Lord, M. Guthold, Fibrin fibers have extraordinary extensibility and elasticity, Science 313 (2006) 634.

[46] N. Bhardwaj, S.C. Kundu, Electrospinning: a fascinating fiber fabrication technique, Biotechnol. Adv. 28 (2010) 325–347.
[47] D. Li, Y.L. Wang, Y.N. Xia, Electrospinning of polymeric and ceramic nanofibers as uniaxially aligned arrays, Nano Lett. 3 (2003) 1167–1171.
[48] C.R. Carlisle, E.A. Sparks, C.D. Loughian, M. Guthold, Strength and failure of fibrin fiber branchpoints, J. Thromb. Haemost. 8 (2010) 1135–1138.
[49] W. Liu, K. Bonin, M. Guthold, An easy and direct method for calibrating AFM lateral force measurements, Rev. Sci. Instrum. 78 (2007) 063707 (063707 pages).
[50] C.T. Lim, E.P.S. Tan, S.Y. Ng, Effects of crystalline morphology on the tensile properties of electrospun polymer nanofibers, Appl. Phys. Lett. 92 (2008).
[51] S.-C. Wong, A. Baji, S. Leng, Effect of fiber diameter on tensile properties of electrospun poly(epsilon-caprolactone), Polymer 49 (2008) 4713–4722.
[52] S.Y. Chew, T.C. Hufnagel, C.T. Lim, K.W. Leong, Mechanical properties of single electrospun drug-encapsulated nanofibres, Nanotechnology 17 (2006) 3880–3891.
[53] F. Croisier, A.S. Duwez, C. Jerome, A.F. Leonard, K.O. van der Werf, P.J. Dijkstra, M.L. Bennink, Mechanical testing of electrospun PCL fibers, Acta Biomater. 8 (2012) 218–224.
[54] D. Dado, M. Sagi, S. Levenberg, A. Zemel, Mechanical control of stem cell differentiation, Regen. Med. 7 (2012) 101–116.
[55] A.J. Engler, S. Sen, H.L. Sweeney, D.E. Discher, Matrix elasticity directs stem cell lineage specification, Cell 126 (2006) 677–689.
[56] S.-Y. Tee, J. Fu, C.S. Chen, P.A. Janmey, Cell shape and substrate rigidity both regulate cell stiffness, Biophys. J. 100 (2011) L25–L27.
[57] M. Guthold, W. Liu, E.A. Sparks, L.M. Jawerth, L. Peng, M. Falvo, R. Superfine, R.R. Hantgan, S.T. Lord, A comparison of the mechanical and structural properties of fibrin fibers with other protein fibers, Cell Biochem. Biophys. 49 (2007) 165–181.
[58] A. Charuchinda, R. Molloy, J. Siripitayananon, N. Molloy, M. Sriyai, Factors influencing the small-scale melt spinning of poly(epsilon-caprolactone) monofilament fibres, Polym. Int. 52 (2003) 1175–1181.